THE JOURNAL OF PHYSICAL CHEMISTRY LETTERS
A JOURNAL OF THE AMERICAN CHEMICAL SOCIETY

pubs.acs.org/JPCL

Letter

Blinking-Based Multiplexing: A New Approach for Differentiating Spectrally Overlapped Emitters

Grace A. DeSalvo, Grayson R. Hoy, Isabelle M. Kogan, John Z. Li, Elise T. Palmer, Emilio Luz-Ricca, Paul Scemama de Gialluly, and Kristin L. Wustholz*

Cite This: J. Phys. Chem. Lett. 2022, 13, 5056−5060

Read Online

ACCESS | Metrics & More | Article Recommendations | Supporting Information

ABSTRACT: Multicolor single-molecule imaging is widely applied to answer questions in biology and materials science. However, most studies rely on spectrally distinct fluorescent probes or time-intensive sequential imaging strategies to multiplex. Here, we introduce blinking-based multiplexing (BBM), a simple approach to differentiate spectrally overlapped emitters based solely on their intrinsic blinking dynamics. The blinking dynamics of hundreds of rhodamine 6G and CdSe/ZnS quantum dots on glass are obtained using the same acquisition settings and analyzed with a change point detection algorithm. Although substantial blinking heterogeneity is observed, the analysis yields a blinking metric with 93.5% classification accuracy. We further show that BBM with up to 96.6% accuracy is achieved by using a deep learning algorithm for classification. This proof-of-concept study demonstrates that a single emitter can be accurately classified based on its intrinsic blinking dynamics and without the need to probe its spectral color.

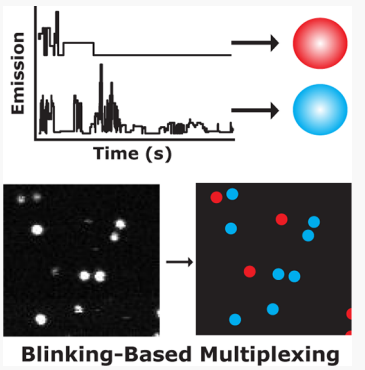

Single-molecule spectroscopy (SMS) and single-molecule localization microscopy (SMLM) have revolutionized biological and materials microscopy by overcoming the diffraction limit of light and elucidating complex structures and processes via "nanoreporting".[1−3] However, many questions can be addressed only by multicolor imaging of multiple fluorescent probes, a capability that remains challenging in many single-molecule experiments. Multicolor imaging is traditionally achieved by labeling several targets within a sample of interest with spectrally distinct probes (e.g., organic dyes, quantum dots, fluorophore-coupled oligonucleotides). Although relatively straightforward to implement, this approach faces several challenges, including a limited number of well-performing probes, spectral cross-talk, and chromatic aberrations. Advances such as spectral demixing, combinatorial detection, multispectral acquisition, and spectrally resolved detection have improved multiplexing performance over the past decade.[4−8] Nonetheless, the requirement for spectrally distinguishable labels limits the number of available probes and ultimately the extent of multiplexing that can be achieved.

An alternative strategy is to eliminate the requirement for spectrally distinct probes altogether. For example, sequential labeling and imaging approaches allow different targets to be sequentially visualized using the same fluorophore, but they are time-intensive and introduce additional drawbacks.[9−11] More recently, Jungmann and co-workers demonstrated that the signal from one fluorophore can be multiplexed by adjusting the transient binding of short dye-labeled (imager) oligonucleotides to their complementary target strands in DNA points accumulation for imaging in nanoscale topography (DNA-PAINT) modality.[12] Although promising, this method uses costly fluorescent oligos and target oligos that are difficult to conjugate to antibodies and introduces nonspecific binding. In this study, we demonstrate an alternative molecular photophysics approach to multiplexing, wherein individual emitters can be differentiated without the need for spectrally distinct probes, additional hardware, sequential imaging, or engineered binding kinetics.

In particular, we introduce blinking-based multiplexing (BBM, Figure 1), a simple and versatile strategy to achieve multiplexed single-molecule detection using the intrinsic blinking dynamics of emitters. Blinking is defined as fluctuations in emission intensity that occur under continuous illumination due to photophysical/chemical transformations. We propose to harness these fluctuations between emissive "on" and non-emissive "off" events that are already being used for localization in several SMLM techniques (e.g., GSDIM, BALM, and SOFI)[13−15] to multiplex spectrally indistinct emitters. The BBM concept holds great potential to expand the palette of available probes and circumvent the time-intensive procedures associated with sequential and DNA-PAINT imaging modalities. Moreover, BBM represents a new take on single-molecule experiments, which has so far restricted

Received: April 26, 2022
Accepted: May 25, 2022
Published: June 2, 2022

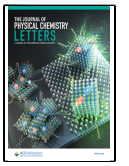

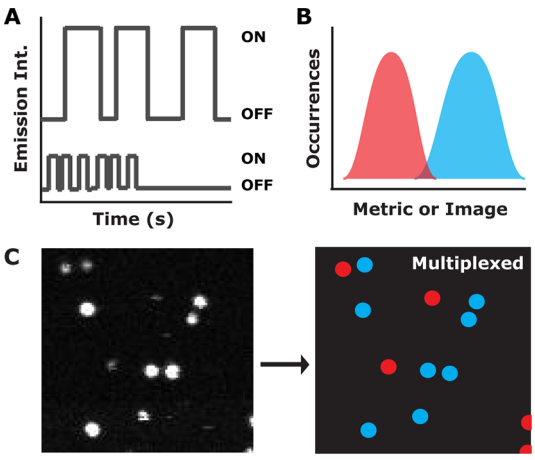

Figure 1. Principle of BBM. (A) Blinking dynamics of spectrally indistinct probes are recorded and (B) classified using either change point detection (CPD) analysis to generate a distinguishable metric or image analysis with deep learning. (C) After classification, the raw intensity image is color coded accordingly.

blinking measurements to the purpose of localization or nanoreporting.

While BBM lifts the need for spectral separation, it requires that the blinking dynamics of emitters are sufficiently distinct, with minimal overlap in their photophysical distributions (Figure 1B). Therefore, for this proof-of-concept study, we selected a model system composed of two commercially available and spectrally overlapped probes (Figure S1) immobilized on glass substrates: rhodamine 6G (R6G) and core−shell CdSe/ZnS quantum dots (QD). R6G and QD are commonly employed in single-molecule experiments and are known to exhibit, *on average*, qualitative differences in blinking. However, several studies have shown the blinking behavior of R6G and QD on glass to be quite dispersed (i.e., with single-emitter events ranging from milliseconds to >100 s in duration and blinking statistics that are lognormally and power-law distributed).[16−19] This photophysical heterogeneity, which originates from dispersive charge-transfer processes arising from both static and dynamic variations in structure and energetics of the emitter and its local environment, is sufficiently broad to be representative of a complex "real world" sample for this initial investigation. To evaluate the BBM concept, we quantify the blinking statistics of hundreds of R6G and QD emitters to develop a classification metric. The accuracy of this metric is then tested by performing experiments on mixed samples of varied R6G and QD composition. As a final step, we use deep learning to perform rapid image classification.

Our goal of multiplexing R6G and QD emitters on the basis of their blinking dynamics alone requires measuring hundreds of emission-time traces and analyzing them using a statistically principled method. We and others have shown that change point detection (CPD) provides a more accurate determination of the statistically significant intensities and event durations within a blinking trace as compared to simple thresholding.[19,20] Based on CPD analysis, a set of blinking statistics is readily determined for each emitter [e.g., the number of distinct emission intensities (N_I), minimum deconvolved intensity (I_{min}), average emission intensity $\langle I \rangle$, average on time $\langle t_{on} \rangle$, average off time $\langle t_{off} \rangle$, and event frequency (number of events per 200 s observation period, ν_E], each of which may be diagnostic for BBM.

Panels A and B of Figure 2 show representative blinking traces of R6G and QD, respectively, on glass obtained using

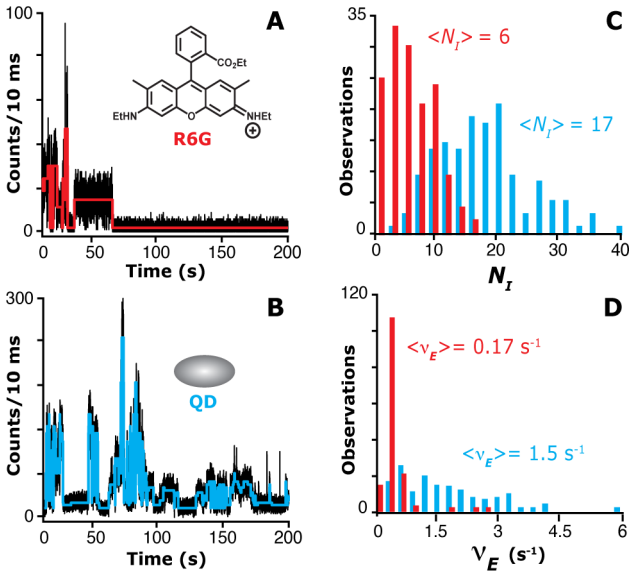

Figure 2. Blinking behavior of (red) R6G and (blue) QD on glass obtained using 532 nm excitation at 1 μW. Representative blinking dynamics of (A) R6G shown with (red line) CPD analysis to yield N_I = 7 and ν_E = 0.2 s^{-1} versus (B) QD blinking that exhibits more intensity fluctuations, consistent with (blue line) CPD analysis to yield N_I = 20 and ν_E = 1.6 s^{-1}. Histograms of (C) N_I and (D) ν_E derived from 148 and 143 blinking measurements of R6G and QD, respectively. $\langle N_I \rangle$ and $\langle \nu_E \rangle$ are smaller for R6G relative to QD, and the corresponding distributions for R6G are also less dispersed.

532 nm laser excitation at 1 μW and a 10 ms bin time. Inspection of the raw emission-time traces reveals differences in blinking behavior, consistent with previous single-emitter studies.[16,21] For example, the QD blinking trace exhibits more intensity fluctuations, brighter emission, and persistent blinking activity as compared to R6G. Indeed, CPD analysis reveals significant differences in blinking statistics. For the R6G molecule, N_I = 7, I_{min} = 3.2 counts, $\langle I \rangle$ = 5.6 counts, $\langle t_{on} \rangle$ = 1.5 s, $\langle t_{off} \rangle$ = 1.6 s, and ν_E = 0.2 s^{-1}, as compared to N_I = 20, I_{min} = 18.3 counts, $\langle I \rangle$ = 40.3 counts, $\langle t_{on} \rangle$ = 0.6 s, $\langle t_{off} \rangle$ = 1.7 s, and ν_E = 1.6 s^{-1} for the QD. Although these individual differences are promising, the full distributions of blinking behavior must be determined.

To this end, we performed blinking measurements of >100 R6G and QD emitters. CPD analysis of the resulting blinking data reveals several key differences in blinking statistics, two of which are shown in Figure 2C,D. The N_I distribution for 148 R6G molecules on glass contains individual values ranging from 1 to 16, with an average value, $\langle N_I \rangle$, of 6.0 ± 0.3, where the error is the standard deviation of the mean. The corresponding N_I distribution for 143 QD ranges from 4 to 38, with $\langle N_I \rangle$ = 17.1 ± 0.6. That is, $\langle N_I \rangle$ is roughly three times larger for QD relative to R6G. Nonetheless, there is significant overlap in the N_I distributions (Figure 2C), meaning that this parameter alone is insufficient to provide for multiplexing. Figure 2D shows the corresponding ν_E distributions for R6G and QD. Again, while the average single-emitter event frequency of QD is nearly an order of magnitude higher

https://doi.org/10.1021/acs.jpclett.2c01252
J. Phys. Chem. Lett. 2022, 13, 5056−5060

relative to R6G, the ν_E distributions are overlapped. As described in the Supporting Information, the other blinking statistics (e.g., $\langle I_{min}\rangle$, $\langle I\rangle$, and $\langle t_{on}\rangle$) yield similar results. To summarize, the average values of the N_I, ν_E, I_{min}, $\langle I\rangle$, and $\langle t_{on}\rangle$ distributions are consistently smaller for R6G as compared to QD, but the histograms are not well-separated between the two emitters (Table S1 and Figure S2).

To amplify the differences between individual blinking statistics and generate multiplexing capability, we developed an empirically derived blinking metric (M) given by

$$M = N_I\, I_{min}\, \nu_E{}^2 \langle I\rangle^2 \langle t_{on}\rangle \quad (1)$$

which is essentially a product of the blinking statistics that best differentiate R6G and QD. This metric is effective here because the average statistics for QD are consistently larger relative to those for R6G. However, it is important to note that depending on the experiment, M might be improved by incorporating both positive and negative exponents into eq 1. As described in the Supporting Information, the blinking statistics are first normalized to the entire R6G and QD data set (n = 291) and then multiplied by 100. Numerous test metrics were evaluated, and eq 1 provided for the best separation between the two emitters in terms of average M values (i.e., $\langle M\rangle = 6 \times 10^5$ for R6G as compared to $\langle M\rangle = 2\times 10^{11}$ for QD) as well as minimal distribution overlap.

Figure 3A presents the M distributions derived from 148 R6G and 143 QD blinking measurements, demonstrating that the vast majority (>90%) of emitters can be accurately classified using a threshold M value of between ~10^3 and ~10^6. To refine the classification threshold, we performed receiver operating characteristic (ROC) curve analysis as described in the Supporting Information. ROC curves are commonly used in clinical diagnostics and more recently in chemical sensing to graphically represent the true positive rate (i.e., TPR: sensitivity) and false positive rate (i.e., FPR: 1 − specificity) of a binary classification system.[22] In this approach, the TPR and FPR are plotted as the threshold for binary classification is varied. Whereas "perfect" classification corresponds to a point at (0,1) that represents no false positives or negatives, random guessing will yield a diagonal line bisecting the ROC space. Thus, the shape of a ROC curve and its corresponding area under the curve (AUC) are used to establish a threshold and measure classification quality.

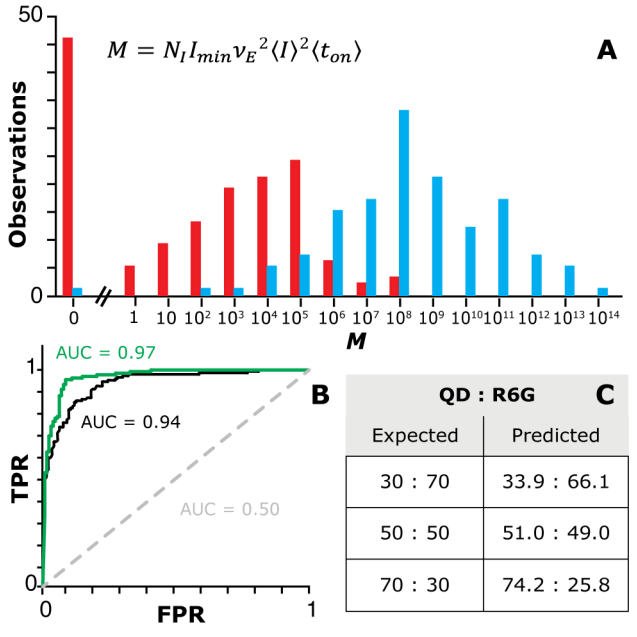

Figure 3. (A) Semilogarithmic histogram of M values compiled from (red) R6G (n = 148) and (blue) QD (n = 143) measurements. (B) ROC curves for (green) M and (black) ν_E classifiers yield AUC values of 0.97 and 0.94, respectively, as compared to the hypothetical case when a classifier cannot distinguish (i.e., AUC = 0.5). (C) Table of expected QD:R6G composition (i.e., 30:70, 50:50, 70:30) versus predicted composition based on BBM obtained from 109, 145, and 97 blinking measurements of mixed QD:R6G samples, respectively.

Figure 3B presents the ROC curves and AUC values for M and ν_E classifiers alongside a hypothetical case corresponding to random guessing (i.e., AUC = 0.5). The classification quality is increased as AUC approaches 1. The ROC plots for M and ν_E yield AUC values of 0.97 and 0.94, respectively. While both parameters provide for excellent classification, M is the better classifier for the system. Furthermore, the ROC curve analysis demonstrates that a threshold M value between 4×10^4 and 8×10^5 is optimal for maximizing true positives (TPR = 0.96) while minimizing false positives (FPR = 0.09). When this double-threshold approach (i.e., $M < 4 \times 10^4$ is classified as R6G, $M > 8 \times 10^5$ is classified as QD) is applied, in the entire blinking data set (n = 291), 93.5% of emitters are correctly classified. To our knowledge, this represents the first demonstration of the BBM concept: a single emitter can be accurately classified based on its intrinsic blinking dynamics (and without the need to probe its spectral color).

Although this approach is accurate, it leaves ~8% of the data unaccounted for (i.e., for emitters with $4 \times 10^4 < M < 8 \times 10^5$). In the process of these analyses, we noted that an experimentalist could often recognize whether a blinking trace appeared to be R6G or a QD *a priori*. For example, whereas QD blinking is often persistent after 150 s (Figure 2B), the blinking dynamics of R6G often (87.2%) terminates in an "off" event (Figure 2A) because of either the population of a long-lived radical cation dark state[16] or molecular photobleaching. Thus, if a BBM practitioner seeks to classify the entire data set, then using both M and this simple visual identifier (i.e., blinking activity after 150 s is classified as QD), will produce a small trade-off in accuracy to 92.5%. If instead users seek to maximize accuracy, then the small subset of emitters would remain unclassified. To further test the BBM approach, we performed blinking measurements of mixed samples of QD and R6G of known composition. Figure 3C shows the predicted compositions resulting from BBM analysis based on M and the aforementioned visual classifier for 109, 145, and 97 blinking measurements of 30:70, 50:50, and 70:30 [QD]:[R6G] mixtures, respectively. The predicted compositions are within 1% to 4% of the expected values.

Inspired by our observation that blinking data can sometimes be visually distinguished, we investigated a deep learning (DL) method for blinking classification. DL is a type of machine learning that has generated substantial attention in chemistry.[23] For the purpose of BBM, DL holds the potential to provide for rapid, accurate emitter classification without the need for M analysis or inputting user-defined features. We implemented a one-dimensional counterpart of residual neural network model, which has been successful for univariate time series classification tasks.[24,25] The entire blinking data set is separated into a training set (n = 232) to adjust the model's parameters in supervised learning, a validation set (n = 35, 15% of the training set), and a test set (n = 59) to quantify model

https://doi.org/10.1021/acs.jpclett.2c01252
J. Phys. Chem. Lett. 2022, 13, 5056−5060

performance. This approach yielded a model with 13 convolutional layers and 1 dense layer, with a maximum classification accuracy of 96.6% on the test set and an average accuracy of 93.2%.

This average accuracy is consistent with the ROC curve for the DL model (Figure S3), which yielded an AUC of 0.96, comparable to the *M*-based classification. When the DL model is applied to blinking traces obtained from mixtures of QD and R6G, the average predicted compositions of the 30:70, 50:50, and 70:30 [QD]:[R6G] samples are 34.4:65.6, 42.1:57.9, and 60.8:39.4, respectively. The predicted compositions are within 5%−9% of the expected compositions. These predictions appear to be less accurate as those achieved via CPD analysis, though still within sampling error, likely because the model is trained on a relatively small data set. Nonetheless, this study demonstrates that DL has the potential to achieve high classification accuracy for BBM, without the need for user-input features or CPD analysis. We anticipate increased fidelity as the training set grows with future experiments and ongoing efforts in data augmentation.

In conclusion, BBM is a powerful new approach to classify individual emitters based solely on their intrinsic blinking dynamics. By measuring and carefully quantifying the blinking dynamics of individual emitters on glass, we demonstrate that accurate binary classification of spectrally overlapped emitters is achieved, even when blinking heterogeneity is substantial. While this study demonstrates proof of the BBM concept, there are several opportunities to expand its capabilities. Notably, this study is performed on glass and with two very different emitters. Modifications to probe structure and sample environment are expected to yield concomitant changes to blinking mechanism and distributions, which will need to be evaluated and controlled, potentially through the use of imaging buffers. Furthermore, our preliminary observations indicate that optimizing the experimental conditions (e.g., excitation power or labeling density) can yield enhanced multiplexing capability. To this end, both fundamental blinking and applied BBM studies of small-molecule probes in various environments and experimental conditions are underway. Ultimately, BBM represents a new take on single-emitter blinking, which holds the potential to expand the palette of available probes and unlock new opportunities in single-molecule imaging and probe design.

METHODS

All glassware and microscope coverslips (Fisher Scientific, 12-545-102), were cleaned in a base bath for 24 h; rinsed with purified, deionized water (Thermo Scientific, Easy Pure II, 18.2 MΩ cm); and dried. R6G (Acros Organics, 99%) and QD (Invitrogen, Qdot 565 ITK carboxyl quantum dots, 8 μM solution in borate buffer) were used as received. Stock solutions were prepared in ultrapure water and sonicated for 1−2 min prior to use. Samples for single-emitter measurements were prepared by spin coating 35 μL of 10^{-9}−10^{-10} M sample onto a clean glass coverslip using a spin coater (Laurell Technologies, WS-400-6NPP-LITE) operating at 3000 rpm. The resulting samples were placed onto a custom aluminum flow cell that was flushed with dry nitrogen during blinking experiments.

Samples for single-molecule studies were placed on a nanopositioning stage (Physik Instrumente, LP E-545) on an inverted confocal microscope (Nikon, TiU). Laser excitation at 532 nm (Spectra Physics, Excelsior) was focused to a diffraction-limited spot using a high numerical aperture (NA) 100× oil-immersion objective (Nikon Plan Fluor, NA = 1.3). An excitation power of 1.05 μW at the sample was used for all single-emitter measurements in order to optimize the emission signal while minimizing molecular photobleaching. Emission from the sample was collected through the objective, passed through an edge filter (Semrock, LP03-532RS-2S), and focused to an avalanche photodiode detector (APD) with a 50 μm aperture (MPD, PDM050CTB) to provide confocal resolution. A *z*-axis microscope lock (Applied Science Instruments, MFC-2000) was used to maintain focus during raster scans. A custom LabView program was used to control the nanopositioning stage and collect corresponding emission intensity using a 30 ms dwell time. The observation of diffraction-limited spots, blinking dynamics, irreversible single-step photobleaching, and concentration dependence of the spot density were used to establish single-emitter detection. Blinking dynamics were acquired using a 10 ms integration time for 200 s.

ASSOCIATED CONTENT

Supporting Information

The Supporting Information is available free of charge at https://pubs.acs.org/doi/10.1021/acs.jpclett.2c01252.

Emission spectra of probes, additional blinking statistics, details on ROC analysis, and additional experimental and computational details (PDF)

Transparent Peer Review report available (PDF)

AUTHOR INFORMATION

Corresponding Author

Kristin L. Wustholz − *Department of Chemistry, William & Mary, Williamsburg, Virginia 23187, United States;* orcid.org/0000-0001-7705-4240; Email: kwustholz@wm.edu

Authors

Grace A. DeSalvo − *Department of Chemistry, William & Mary, Williamsburg, Virginia 23187, United States*

Grayson R. Hoy − *Department of Chemistry, William & Mary, Williamsburg, Virginia 23187, United States*

Isabelle M. Kogan − *Department of Chemistry, William & Mary, Williamsburg, Virginia 23187, United States*

John Z. Li − *Department of Chemistry, William & Mary, Williamsburg, Virginia 23187, United States*

Elise T. Palmer − *Department of Chemistry, William & Mary, Williamsburg, Virginia 23187, United States*

Emilio Luz-Ricca − *Department of Chemistry, William & Mary, Williamsburg, Virginia 23187, United States;* orcid.org/0000-0002-4180-4123

Paul Scemama de Gialluly − *Department of Chemistry, William & Mary, Williamsburg, Virginia 23187, United States*

Complete contact information is available at: https://pubs.acs.org/10.1021/acs.jpclett.2c01252

Notes

The authors declare no competing financial interest.

ACKNOWLEDGMENTS

This work was supported by the National Science Foundation (CHE-2102099).

REFERENCES

(1) Möckl, L.; Moerner, W. E. Super-Resolution Microscopy with Single Molecules in Biology and Beyond-Essentials, Current Trends, and Future Challenges. *J. Am. Chem. Soc.* **2020**, *142* (42), 17828−17844.

(2) Willets, K. A.; Wilson, A. J.; Sundaresan, V.; Joshi, P. B. Super-Resolution Imaging and Plasmonics. *Chem. Rev.* **2017**, *117* (11), 7538−7582.

(3) Patterson, G.; Davidson, M.; Manley, S.; Lippincott-Schwartz, J. Superresolution Imaging Using Single-Molecule Localization. *Annu. Rev. Phys. Chem.* **2010**, *61* (1), 345−367.

(4) Grußmayer, K. S.; Geissbuehler, S.; Descloux, A.; Lukes, T.; Leutenegger, M.; Radenovic, A.; Lasser, T. Spectral Cross-Cumulants for Multicolor Super-Resolved SOFI Imaging. *Nat. Commun.* **2020**, *11* (1), 1−8.

(5) Lubeck, E.; Cai, L. Single-Cell Systems Biology by Super-Resolution Imaging and Combinatorial Labeling. *Nat. Methods* **2012**, *9* (7), 743−748.

(6) Bates, M.; Dempsey, G. T.; Chen, K. H.; Zhuang, X. Multicolor Super-Resolution Fluorescence Imaging via Multi-Parameter Fluorophore Detection. *ChemPhysChem* **2012**, *13* (1), 99−107.

(7) Valm, A. M.; Cohen, S.; Legant, W. R.; Melunis, J.; Hershberg, U.; Wait, E.; Cohen, A. R.; Davidson, M. W.; Betzig, E.; Lippincott-Schwartz, J. Applying Systems-Level Spectral Imaging and Analysis to Reveal the Organelle Interactome. *Nature* **2017**, *546* (7656), 162−167.

(8) Zhang, Z.; Kenny, S. J.; Hauser, M.; Li, W.; Xu, K. Ultrahigh-Throughput Single-Molecule Spectroscopy and Spectrally Resolved Super-Resolution Microscopy. *Nat. Methods* **2015**, *12* (10), 935−938.

(9) Tam, J.; Cordier, G. A.; Borbely, J. S.; Álvarez, Á. S.; Lakadamyali, M. Cross-Talk-Free Multi-Color Storm Imaging Using a Single Fluorophore. *PLoS One* **2014**, *9* (7), e101772.

(10) Valley, C. C.; Liu, S.; Lidke, D. S.; Lidke, K. A. Sequential Superresolution Imaging of Multiple Targets Using a Single Fluorophore. *PLoS One* **2015**, *10* (4), e0123941.

(11) Schnitzbauer, J.; Strauss, M. T.; Schlichthaerle, T.; Schueder, F.; Jungmann, R. Super-Resolution Microscopy with DNA-PAINT. *Nat. Protocols* **2017**, *12* (6), 1198−1228.

(12) Wade, O. K.; Woehrstein, J. B.; Nickels, P. C.; Strauss, S.; Stehr, F.; Stein, J.; Schueder, F.; Strauss, M. T.; Ganji, M.; Schnitzbauer, J.; et al. 124-Color Super-Resolution Imaging by Engineering DNA-PAINT Blinking Kinetics. *Nano Lett.* **2019**, *19* (4), 2641−2646.

(13) Fölling, J.; Bossi, M.; Bock, H.; Medda, R.; Wurm, C. A.; Hein, B.; Jakobs, S.; Eggeling, C.; Hell, S. W. Fluorescence Nanoscopy by Ground-State Depletion and Single-Molecule Return. *Nat. Methods* **2008**, *5* (11), 943−945.

(14) Burnette, D. T.; Sengupta, P.; Dai, Y.; Lippincott-Schwartz, J.; Kachar, B. Bleaching/Blinking Assisted Localization Microscopy for Superresolution Imaging Using Standard Fluorescent Molecules. *Proc. Natl. Acad. Sci. U.S.A.* **2011**, *108* (52), 21081−21086.

(15) Gallina, M. E.; Xu, J.; Dertinger, T.; Aizer, A.; Shav-Tal, Y.; Weiss, S. Resolving the Spatial Relationship between Intracellular Components by Dual Color Super Resolution Optical Fluctuations Imaging (SOFI). *Opt. Nano.* **2013**, *2* (1), 1−9.

(16) Wong, N. Z.; Ogata, A. F.; Wustholz, K. L. Dispersive Electron-Transfer Kinetics from Single Molecules on TiO_2 Nanoparticle Films. *J. Phys. Chem. C* **2013**, *117* (41), 21075−21085.

(17) Lynch, P. G.; Richards, H.; Wustholz, K. L. Unraveling the Excited-State Dynamics of Eosin Y Photosensitizers Using Single-Molecule Spectroscopy. *J. Phys. Chem. A* **2019**, *123* (13), 2592−2600.

(18) Margolin, G.; Protasenko, V.; Kuno, M.; Barkai, E. Photon Counting Statistics for Blinking CdSe-ZnS Quantum Dots: A Lévy Walk Process. *J. Phys. Chem. B* **2006**, *110* (38), 19053−19060.

(19) Kopera, K. M.; Tuckman, H. G.; Hoy, G. R.; Wustholz, K. L. Origin of Kinetic Dispersion in Eosin-Sensitized TiO_2: Insights from Single-Molecule Spectroscopy. *J. Phys. Chem. C* **2021**, *125* (43), 23634−23645.

(20) Watkins, L. P.; Yang, H. Detection of Intensity Change Points in Time-Resolved Single-Molecule Measurements. *J. Phys. Chem. B* **2005**, *109* (1), 617−628.

(21) Cordones, A. A.; Bixby, T. J.; Leone, S. R. Evidence for Multiple Trapping Mechanisms in Single CdSe/ZnS Quantum Dots from Fluorescence Intermittency Measurements over a Wide Range of Excitation Intensities. *J. Phys. Chem. C* **2011**, *115* (14), 6341−6349.

(22) Reaser, B. C.; Wright, B. W.; Synovec, R. E. Using Receiver Operating Characteristic Curves to Optimize Discovery-Based Software with Comprehensive Two-Dimensional Gas Chromatography with Time-of-Flight Mass Spectrometry. *Anal. Chem.* **2017**, *89* (6), 3606−3612.

(23) Mater, A. C.; Coote, M. L. Deep Learning in Chemistry. *J. Chem. Inf. Model.* **2019**, *59*, 2545−2559.

(24) He, K.; Zhang, X.; Ren, S.; Sun, J. Deep Residual Learning for Image Recognition. *Proceedings of the IEEE Computer Society Conference on Computer Vision and Pattern Recognition* **2016**, *2016* (Decem), 770−778.

(25) Ismail Fawaz, H.; Forestier, G.; Weber, J.; Idoumghar, L.; Muller, P. A. Deep Learning for Time Series Classification: A Review. *Data Mining Knowledge Discovery* **2019**, *33* (4), 917−963.

https://doi.org/10.1021/acs.jpclett.2c01252
J. Phys. Chem. Lett. 2022, 13, 5056−5060